PHYSICAL REVIEW D **87,** 095008 (2013)

Probing color octet electrons at the LHC

Tanumoy Mandal[1,*] and Subhadip Mitra[2,†]

[1]*The Institute of Mathematical Sciences, Chennai, Tamil Nadu 600 113, India*

[2]*Laboratoire de Physique Théorique, CNRS-UMR 8627, Université Paris-Sud 11, F-91405 Orsay Cedex, France*

(Received 13 March 2013; published 14 May 2013)

Models with quark and lepton compositeness predict the existence of colored partners of the Standard Model leptons. In this paper we study the LHC phenomenology of a charged colored lepton partner, namely the color octet electron, e_8, in an effective theory framework. We explore various mechanisms for resonant production of e_8's. With the pair production channel, the 14 TeV LHC can probe e_8's with masses up to 2.5 TeV (2.8 TeV) with 100 fb^{-1} (300 fb^{-1}) of integrated luminosity. A common feature in all the resonant production channels is the presence of two high-p_T electrons and at least one high-p_T jet in the final state. Using this feature, we implement a search method where the signal is a combination of pair and single production events. This method has potential to increase the LHC's reach significantly. Using the combined signal, we estimate the LHC discovery potential for the e_8's. Our analysis shows that the LHC with 14 TeV center-of-mass energy and 100 fb^{-1} (300 fb^{-1}) of integrated luminosity can probe e_8's with masses up to 3.4 TeV (4 TeV) for the compositeness scale of 5 TeV.

DOI: 10.1103/PhysRevD.87.095008 PACS numbers: 12.60.Rc, 14.80.−j

I. INTRODUCTION

All the experimental outcomes so far indicate that the Standard Model (SM) is the correct effective theory of elementary particles for energies below the TeV scale. If the recently discovered Higgs-like boson at the Large Hadron Collider (LHC) at CERN is confirmed to be the SM Higgs, it will complete the experimental verification of the particle spectrum of the SM [1,2]. However, despite its spectacular success with the experiments, there remain some issues like the hierarchy problems, fermion family replication, etc., that are not properly addressed in the SM. Many theoretical attempts have been made to resolve these issues. Beyond-the-SM (BSM) alternatives like supersymmetry, extra dimensions, and quark-lepton compositeness are some well-known examples. Many of the BSM theories predict the existence of new particles with masses near the TeV scale. Two detectors of the LHC, namely ATLAS and CMS, are presently looking for the signatures of some of these new particles.

Of the various BSM scenarios, the quark-lepton composite models assume that the SM particles may not be fundamental, and just as the proton has constituent quarks, they are actually bound states of substructural constituents (preons) [3]. These constituents are visible only beyond a certain energy scale known as the compositeness scale. A typical consequence of quark-lepton compositeness is the appearance of colored particles with nonzero lepton numbers (leptogluons, leptoquarks) and excited leptons, etc. Some composite models naturally predict the existence of leptogluons (l_8) [3–9] that are color octet fermions with nonzero lepton numbers. Several studies on the collider searches of leptoquarks and excited fermions can be found in the literature [10–12], but there are only a few similar studies on l_8's. Various signatures of color octet leptons at different colliders were investigated in some earlier papers [13–18]. Recently some important production processes of the l_8 have been analyzed for future colliders like the Large Hadron-electron Collider (LHeC), the International Linear Collider (ILC) and the Compact Linear Collider (CLiC) [19,20]. We briefly review the limits on (charged) color octet leptons available in the literature. The lower mass limit of color octet charged leptons quoted in the latest Particle Data Book [21] is only 86 GeV. This limit is from the 23-year-old Tevatron data [22] from the pair production channel. A mass limit of $M_{l_8} > \mathcal{O}(110)$ GeV from the direct pair production via color interactions has been derived from $p\bar{p}$ collider data in Ref. [23]. Lower limits on the leptogluons' masses were derived by the JADE Collaboration from the t-channel contribution to the total hadronic cross section, $M_{l_8} \gtrsim (240\ \text{GeV})^3/4\Lambda^2$ (where Λ is the compositeness scale), and from direct production via one photon exchange, $M_{l_8} \gtrsim 20$ GeV [24]. In Ref. [25], the compositeness scale $\Lambda \lesssim 1.8$ TeV was excluded at the 95% confidence level (C.L.) for $M_{l_8} \simeq 100$ GeV and $\Lambda \lesssim 200$ GeV for $M_{l_8} \simeq 200$ GeV. It is also mentioned in Ref. [17] that the D0 cross-section bounds on $eejj$ events exclude leptogluons with masses up to 200 GeV and could naively place the constraint $M_{l_8} \gtrsim 325$ GeV.

In this paper we study the LHC discovery potential for a generic color octet partner of a charged lepton, namely the color octet electron, e_8. Although in this paper we consider only color octet electrons, our results are applicable for the color octet partner of the muon, i.e., μ_8 also. The paper is organized as follows: in Sec. II we display the interaction Lagrangian and decay width of e_8. In Sec. III we discuss various e_8 production processes at the LHC. In Sec. IV we

*tanumoy@imsc.res.in

†subhadip.mitra@th.u-psud.fr

discuss the LHC reach for e_8's. Finally, in Sec. V we summarize and offer our conclusions.

II. THE LAGRANGIAN

Assuming lepton flavor conservation, we consider a general Lagrangian for the color octet electrons including terms allowed by the gauge symmetries of the SM:

$$\mathcal{L} = \bar{e}_8^a i\gamma^\mu(\partial_\mu \delta^{ac} + g_s f^{abc} G^b) e_8^c - M_{e_8} \bar{e}_8^a e_8^a + \mathcal{L}_{\rm int}. \quad (1)$$

For simplicity, we have ignored the terms with electroweak couplings. The interaction part ($\mathcal{L}_{\rm int}$) contains all the higher-dimensional operators. In this paper we consider only the following dimension-5 terms that contain the interaction between ordinary electrons and color octet ones [21][1]:

$$\mathcal{L}_{\rm int} = \frac{g_s}{2\Lambda} G^a_{\mu\nu}[\bar{e}_8^a \sigma^{\mu\nu}(\eta_L e_L + \eta_R e_R)] + \text{H.c.} \quad (2)$$

Here $G^a_{\mu\nu}$ is the gluon field strength tensor, Λ is the scale below which this effective theory is valid and $\eta_{L/R}$ are the chirality factors. Since electron chirality conservation implies $\eta_L \eta_R = 0$, we set $\eta_L = 1$ and $\eta_R = 0$ in our analysis.

From the interaction Lagrangian given in Eq. (2), we see that an e_8 can decay to a gluon and an electron (two-body decay mode), i.e., $e_8 \to eg$, or two gluons and an electron (three-body decay mode), i.e., $e_8 \to egg$ (via the $e_8 egg$ vertex). However, compared to the $e_8 eg$ decay rate, the three-body decay rate is suppressed by an extra power of α_s and phase space suppression. If one includes dimension-6 or higher-dimensional terms in the Lagrangian, then in general, e_8 can have other many body decay modes, like $e_8 \to eqq$ via a four-fermion $e_8 eqq$ vertex. However, these many-body decays will be much more suppressed than the two-body decay. Hence, in this paper, we focus only on the dominant two-body decay mode. With $\eta_L = 1$ and $\eta_R = 0$, the decay width of e_8 can be written as

$$\Gamma_{e_8} = \frac{\alpha_s(M_{e_8}) M_{e_8}^3}{4\Lambda^2}. \quad (3)$$

[1]There are actually more dimension-5 operators allowed by the gauge symmetries and lepton number conservation, like

$$\frac{C_8}{\Lambda} i f^{abc} \bar{e}_8^a G^b_{\mu\nu} \sigma^{\mu\nu} e_8^c + \frac{C_1}{\Lambda} \bar{e}_8^a B_{\mu\nu} \sigma^{\mu\nu} e_8^a.$$

However, these terms lead to momentum-dependent $e_8 e_8 V$ vertices (form factors). Moreover, the octet term can lead to an $e_8 e_8 gg$ vertex which can affect the production cross section. We assume the unknown coefficients associated with these terms are negligible.

III. PRODUCTION AT THE LHC

In this section, we discuss various production mechanisms of e_8's at the LHC and present the production cross sections for different channels. To obtain the cross sections, we have first implemented the Lagrangian of Eq. (1) in FEYNRULES version 1.6.0 [26] to generate Universal FeynRules Output (UFO)-format [27] model files suitable for MADGRAPH5 [28] that we have used to estimate the cross sections. We have used CTEQ6L1 parton distribution functions (PDFs) [29] for all our numerical computations.

At a hadron collider like the LHC, resonant productions of e_8's can occur via gg-, gq- and qq-initiated processes, where q can be either a light quark or a bottom quark. The gluon PDF dominates at the low-x region, whereas the quark PDFs take over at the high-x region. Thus, depending on M_{e_8}, all of the gg-, gq- and qq-initiated processes can contribute significantly to the production of e_8's at the LHC.

For the resonant production e_8's at colliders, two separate channels are generally considered in the literature—one is the pair production [17,18], and the other is the single production of e_8 [13–16,19]. In general, pair production of a colored particle is considered mostly model independent. This is because the universal strong coupling constant g_S controls the dominant pair production processes, unlike the single production processes, where the cross section depends more on various model parameters like couplings and scales, etc. However, as we shall see, for e_8's, the t-channel electron exchange diagrams can contribute significantly to the pair production, making it more model dependent.

A. Pair production ($gg, qq \to e_8 e_8$)

At the LHC, pair production of e_8's is gg- or qq-initiated—see Fig. 1, where we have shown the parton-level Feynman diagrams for this channel. Of these, only the electron exchange diagram, shown in Fig. 1(d), contains the Λ-dependent gee_8 vertex. In Fig. 2, we show the $pp \to e_8 e_8$ cross section as a function of M_{e_8} for two different choices of Λ, $\Lambda = M_{e_8}$ and $\Lambda = 5$ TeV, at the 14 TeV LHC. In Fig. 3, we have plotted $\delta\sigma$ as a function of Λ to show the dependence of the pair production cross section on Λ for $M_{e_8} = 1$ and 2 TeV, where $\delta\sigma$ is a measure of the contribution of the electron exchange diagram and is defined as

$$\delta\sigma(\Lambda) = \sigma(\Lambda) - \sigma(\Lambda \to \infty). \quad (4)$$

As Λ increases, the contribution coming from the electron exchange diagrams decreases and for $\Lambda \gg M_{e_8}$ becomes negligible. So the pair production is model independent only for very large Λ.

After being produced as pairs at the LHC, each e_8 decays into an electron (or a positron) and a gluon at the parton level, i.e.,

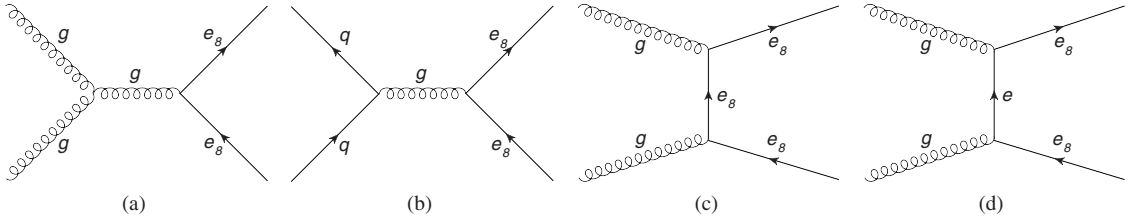

FIG. 1. Parton-level Feynman diagrams for $pp \to e_8 e_8$ processes at the LHC.

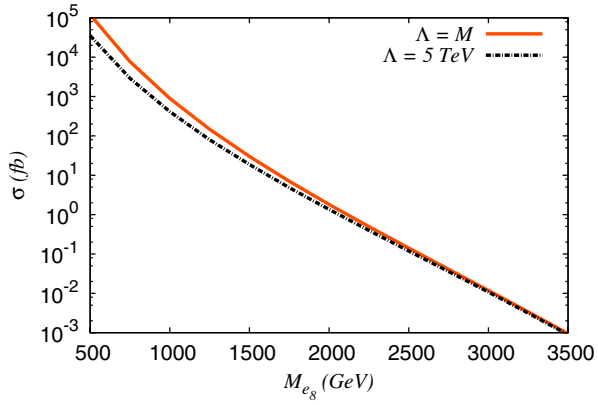

FIG. 2 (color online). The cross sections for $pp \to e_8 e_8$ as a function of M_{e_8} for $\Lambda = M_{e_8}$ and $\Lambda = 5$ TeV at the 14 TeV LHC.

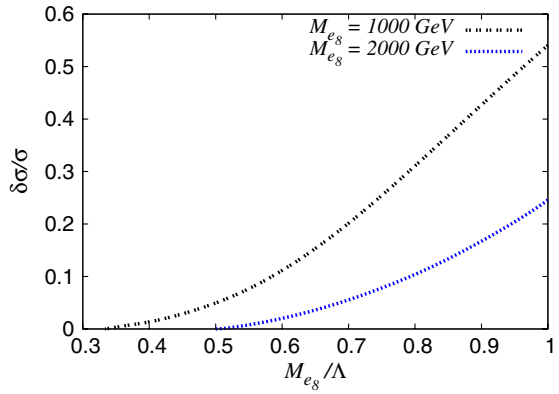

FIG. 3 (color online). Dependence of $\delta\sigma/\sigma$ [defined in Eq. (4)] on M_{e_8}/Λ for $M_{e_8} = 1$ and 2 TeV at the 14 TeV LHC.

$$gg/qq \to e_8 e_8 \to eejj.$$

For large M_{e_8}, these two jets and the lepton pair will have high p_T. This feature can be used to isolate the e_8 pair production events from the SM backgrounds at the LHC.

B. Two-body single production ($gg, qq \to e_8 e$)

The two-body single production channel where an e_8 is produced in association with an electron can have either gg or qq initial states, as shown in Fig. 4. This channel is model dependent, as each Feynman diagram for the $pp \to e_8 e$ process contains a Λ-dependent vertex. In Fig. 5, we show the $pp \to e_8 e$ cross sections as a function of M_{e_8} with $\Lambda = M_{e_8}$ and 5 and 10 TeV at the 14 TeV LHC.

As the e_8 decays, this process gives rise to an eej final state at the parton level. The e and the j produced from the decay of the e_8 have high p_T. The other e also possesses very high p_T as it balances against the massive e_8.

C. Three-body single production ($gg, gq, qq \to e_8 e j$)

Apart from the pair and the two-body single productions, we also consider single production of an e_8 in association with an electron and a jet. The $pp \to e_8 ej$ process includes three different types of diagrams, as follows:

(1) The diagrams where the ej pair is coming from another e_8. Though there are three particles in the final state, this type of diagram effectively corresponds to a two-body pair production process.
(2) The two-body single production ($pp \to e_8 e$) process with a jet radiated from the initial state (ISR) or final state (FSR) or intermediate virtual particles can lead to an $e_8 ej$ final state.
(3) A new set of diagrams that are different from the two types of diagrams mentioned above. These new channels can proceed through gg, qq and gq initial states, as shown in Fig. 6.

This new set of diagrams has not been considered so far in the literature. It is difficult to compute the total contribution of these diagrams in a straightforward manner with a leading-order parton-level matrix element calculation, because of the presence of soft radiation jet emission diagrams. In order to get an estimation of the contribution of these new diagrams without getting into the complicacy of evaluating the soft jet emission diagrams, here, in this section, we present the cross section only for the gq-initiated processes, i.e., $gq \to e_8 ej$, since the first and the second types of diagrams cannot be initiated by a gq state. In Fig. 7, we show the cross section of the $gq \to e_8 ej$ process along with the $pp \to e_8 e_8$ and the $pp \to e_8 e$ processes. We find that the cross sections even for the gq-initiated subset can be comparable to the $pp \to e_8 e_8/e_8 e$ processes for large M_{e_8}, despite the facts that these new diagrams have three-body final states and that they are suppressed by one extra power of the coupling

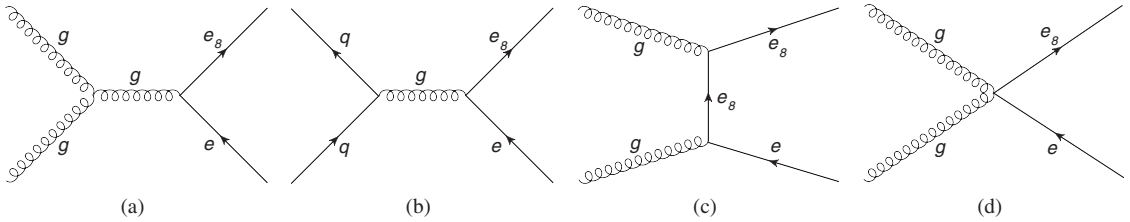

FIG. 4. Parton-level Feynman diagrams for $pp \to e_8 e$ processes at the LHC.

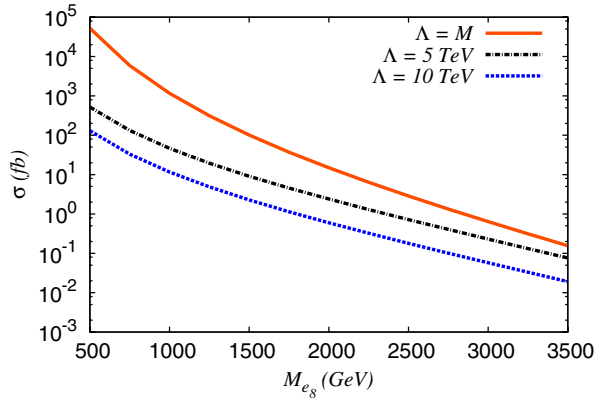

FIG. 5 (color online). The cross sections for $pp \to e_8 e$ as a function of M_{e_8} for $\Lambda = M_{e_8}$, 5 and 10 TeV at the 14 TeV LHC.

(either g_S or g_S/Λ) compared to the two-body single and pair production processes. However, since there is one less e_8 compared to the pair production process, depending on the coupling, the three-body phase space of the single production can be comparable to or even larger than the two-body phase space of the pair production for large M_{e_8}.

After the e_8 decay, the three-body single production process is characterized by an $eejj$ final state like the pair production. However, unlike the pair production, here one of the jets can have a low transverse momentum.

D. Indirect production ($gg \to ee$)

So far we have considered only resonant production of e_8's. However, a t-channel exchange of the e_8 can convert a gluon pair to an electron-positron pair at the LHC (Fig. 8).

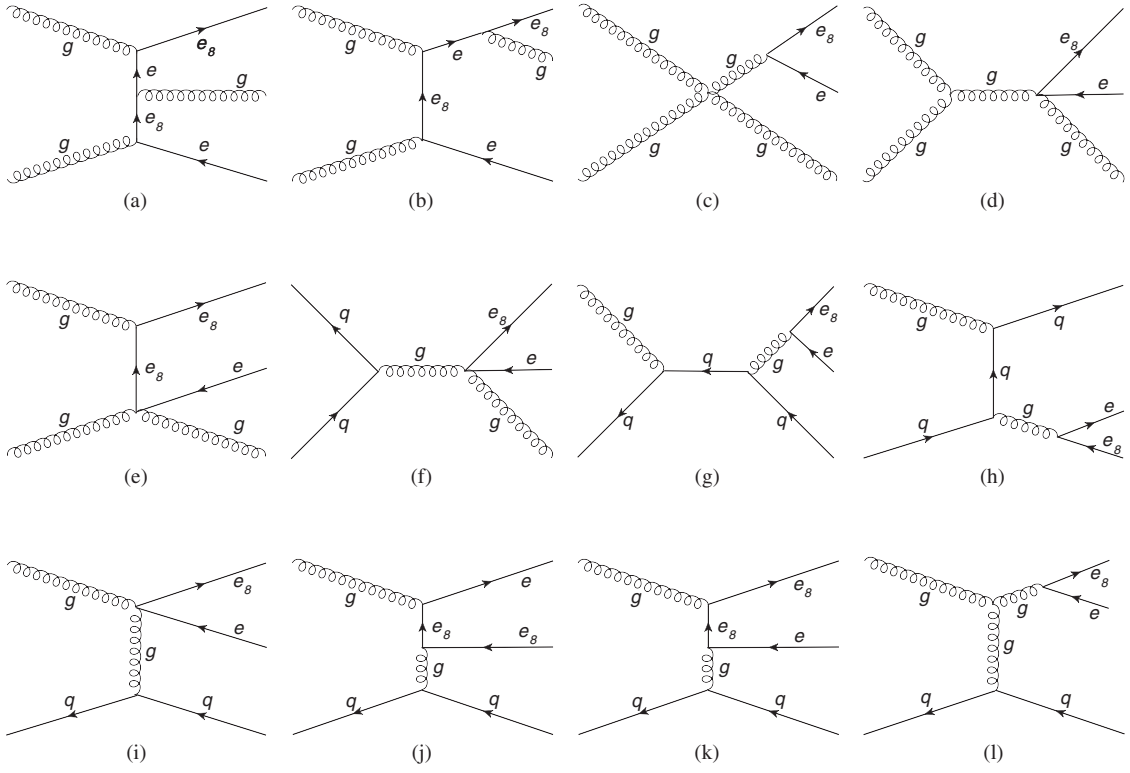

FIG. 6. Parton-level Feynman diagrams for $pp \to e_8 ej$ processes of the third type at the LHC.

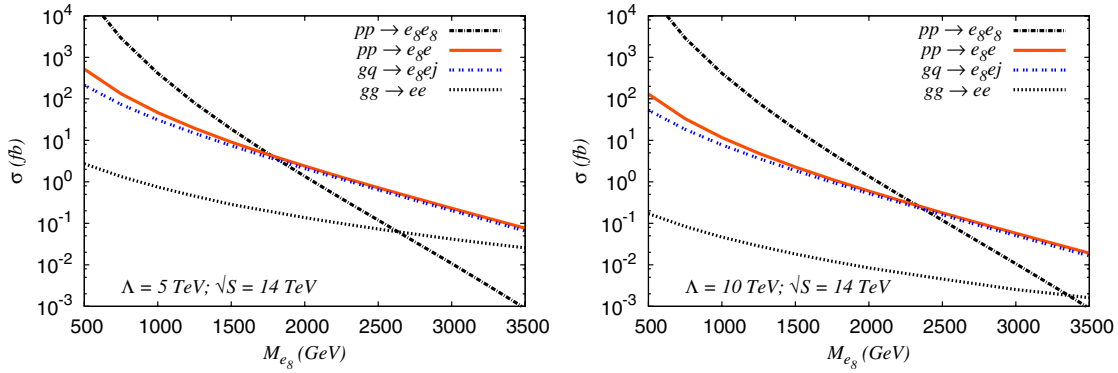

FIG. 7 (color online). Cross sections for $pp \to e_8 e_8$, $pp \to e_8 e$, $gq \to e_8 ej$ and $gg \xrightarrow{e_8} ee$ processes for $\Lambda = 5$ and 10 TeV at the 14 TeV LHC. The $\sigma(gq \to e_8 ej)$ is computed with the following kinematical cuts: $p_T(j) > 25$ GeV and $|y(j)| < 2.5$.

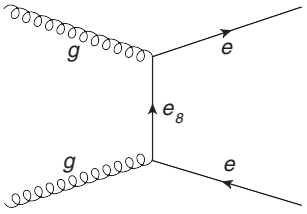

FIG. 8. Parton-level Feynman diagram for indirect production of e_8's at the LHC.

Similar indirect productions in the context of future linear colliders such as the ILC and CLiC have been analyzed in Ref. [20]. Indirect production is less significant, because the amplitude is proportional to $1/\Lambda^2$. Moreover, at the LHC this is also color suppressed, because of the color singlet nature of the final states. In Fig. 7, we also show the cross section of the indirect production process at the LHC.

IV. LHC DISCOVERY POTENTIAL

From Fig. 7 we see that for small M_{e_8}, the pair production cross section is larger than the other channels. As M_{e_8} increases, it decreases rapidly due to phase space suppression, and the single production channels (both the two-body and the three-body) take over the pair production (the crossover point depends on Λ). Hence, if Λ is not too high, the single production channels will have better reach than the pair production channel and so, to estimate the LHC discovery reach, we consider both the pair and the single production channels. However, while estimating for the single production channels, we have to remember that because of the radiation jets, it will be difficult to separate the two-body and the three-body single productions at the LHC. So, in this paper, we consider a selection criterion that combines events from all the production processes at the LHC.

A. Combined signal

To design the selection criterion mentioned above, we first note some of the characteristics of the final states of the resonant production processes[2]:

(1) Process $pp \to e_8 e_8 \to (eg)(eg)$ has two high-p_T electrons and two high-p_T jets in the final state.
(2) Process $pp \to e_8 e \to (eg)e$ has two high-p_T electrons and one high-p_T jet in the final state.
(3) Process $pp \to e_8 ej \to (eg)ej$ has two high-p_T electrons and at least one high-p_T jet in the final state.

All these processes have one common feature: they have two high-p_T electrons and a high-p_T jet in the final state. Hence, if we demand that the signal events should have two high-p_T electrons and at least one high-p_T jet, we can capture events from all the above mentioned production processes. To estimate the number of signal events that pass the above selection criterion, we combine the events from all the production channels mentioned in the previous section. However, as already pointed out, it is difficult to estimate the number of signal events with only a matrix element (ME)-level Monte Carlo computation due to the presence of soft radiation jets. Hence, we use the MADGRAPH ME generator to compute the hard part of the amplitude and PYTHIA6 (via the MADGRAPH5-PYTHIA6 interface) for parton showering. We also match the matrix element partons with the parton showers to estimate the inclusive signal without double counting (see the Appendix for more details on the matched signal).

B. SM backgrounds

With the selection criterion mentioned above, the SM backgrounds are characterized by the presence of two opposite-sign electrons and at least one jet in the final state. At the LHC, the main source of e^+e^- pairs (with high p_T)

[2]We focus on the resonant productions, because as we saw, the indirect production is less significant at the LHC.

TABLE I. The main SM backgrounds to the combined production of e_8's obtained after applying the Basic cuts (see text for definition).

Process	Cross section (fb)
$Z + nj$	2.11E4
tt	1.95E3
tW	132.15
WW	7.51
Total	2.32E4

is the Z decay.[3] Hence, we compute the inclusive Z production as the main background. Here, too, we compute this by matching the matrix element partons of $Z + n$ jets ($n = 0, 1, 2, 3$) processes[4] with the parton showers using the shower k_T scheme [30]. For the background, we also consider some potentially significant processes to produce e^+e^- pairs:

$$pp \to tt \to (bW)(bW) \to (be\nu_e)(be\nu_e),$$
$$pp \to tW \to bWW \to (be\nu_e)(e\nu_e),$$
$$pp \to WW \to (e\nu_e)(e\nu_e).$$

Note that all these processes have missing energy because of the ν_e's in the final state. In Table I, we show the relative contributions of these backgrounds generated with some basic kinematical cuts (to be described shortly) on the final states. As mentioned, we see in Table I that the inclusive Z contribution overwhelms the other background processes.

C. Kinematical cuts

In Fig. 9(a), we display the p_T distributions of e's from the combined signal and the inclusive Z production, respectively. For the signal, we have chosen $M_{e_8} = 2$ TeV and $\Lambda = 5$ TeV. As expected, the distribution for the e coming from the background has a peak at about $M_Z/2$, but there is no such peak for the signal. We can also see the difference between the p_T distributions of the leading p_T jets for the signal and the background in Fig. 9(b). We also display the distributions of $M(e^+, e^-)$ [see Fig. 9(c)] and $M(e^-, j_1)$ [see Fig. 9(d)] (where j_1 denotes the leading p_T jet), which show very different natures for the signal and the background.

Motivated by these distributions, we construct some kinematical cuts to separate the signal from the background:

(1) *Basic cuts*
For $x, y = e^+, e^-, j_1, j_2$ (j_1 and j_2 denote the first two of the p_T-ordered jets, respectively)
(a) $p_T(x) > 25$ GeV
(b) Rapidity, $|\eta(x)| < 2.5$
(c) Radial distance, $\Delta R(x, y)_{x \neq y} \geq 0.4$

(2) *Discovery cuts*
(a) All the *Basic* cuts
(b) $p_T(e^+/e^-) > 150$ GeV; $p_T(j_1) > 100$ GeV
(c) $M(e^+, e^-) > 150$ GeV
(d) For at least one combination of (e, j_i): $|M(e, j_i) - M_{e_8}| \leq 0.2 M_{e_8}$, where $e = e^+$ or e^- and $j_i = j_1$ or j_2.

The cut on $M(e^+, e^-)$ can remove the Z-inclusive background almost completely. For our estimation of the LHC discovery reach, we also use the cut on $M(e, j_i)$ to demand that either of the electrons reconstruct to an e_8 when combined with any one of j_1 or j_2. Although this cut involves an unknown parameter, namely M_{e_8}, it can be implemented in the actual experiment by performing a scan of M_{e_8} over a range (say, 0.5 to 4 TeV). While scanning, for each value of M_{e_8}, one can apply this cut on all the events. If e_8 exists within the scanned region, it will lead to an excess of events (compared to the SM) around the actual value of M_{e_8}. We find that the Discovery cuts can reduce the SM background drastically. Especially for higher M_{e_8}, the background becomes much smaller compared to the signal, making it essentially background free.[5] In Table II, we show the signal with the above two cuts applied.

D. LHC reach with combined signal

We define the luminosity requirement for the discovery of color octet electrons at the LHC as the following:

$$L_D = \text{Max}(L_5, L_{10}), \tag{5}$$

where L_5 denotes the luminosity required to attain 5σ statistical significance for $S/\sqrt{B}$, and L_{10} is the luminosity required to observe ten signal events. We show L_D as a function of M_{e_8} for the Discovery cuts in Fig. 10 for $\Lambda = 5$ and 10 TeV at the 14 TeV LHC. In Fig. 10, we also plot the L_D using only the pair production process. To estimate the pair production from the combined signal, we apply a set of kinematical cuts almost identical to the Discovery cuts, except that now we demand that the two electrons and the two leading p_T jets reconstruct to two e_8's instead of one:

[3]Here we do not include e^+e^- pairs that come from γ^*. However, as we shall demand very high p_T for both the electrons, this background becomes negligible and will not affect our results too much.

[4]Here $pp \to Zjj$ includes the processes where the jets are coming from a W or a Z.

[5]For $M_{e_8} = 0.5$ TeV (1 TeV), we estimate the total SM background with the Discovery cuts at the 14 TeV LHC to be about 4 fb (0.3 fb). Although these numbers are only rough estimates for the actual SM backgrounds (as, e.g., we do not consider the effect of any loop-induced diagrams), they indicate the SM backgrounds become very small compared to the signal (see Table II) after the Discovery cuts.

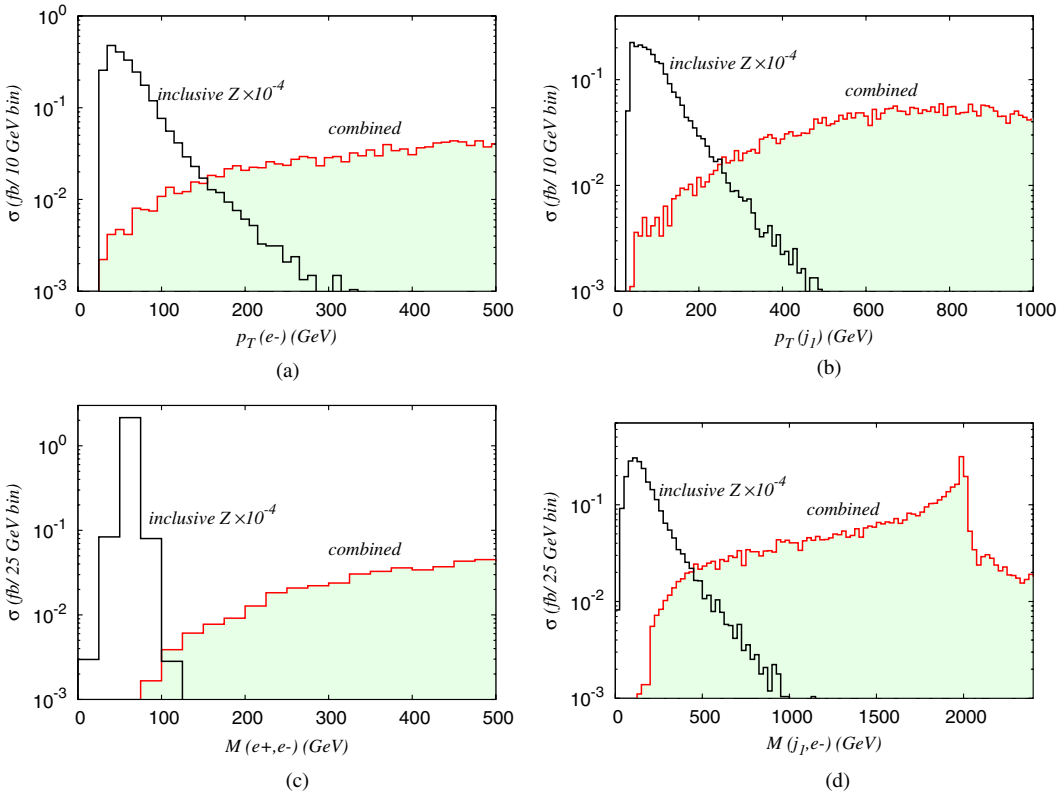

FIG. 9 (color online). Comparison between various distributions for the combined signal with $M_{e_8} = 2$ TeV ($\Lambda = 5$ TeV) and the inclusive Z background for the 14 TeV LHC—(a) p_T distribution of the electron, (b) p_T distribution of the leading p_T jet, (c) invariant mass distribution of the e^+e^- pair and (d) invariant mass distribution of the electron and the leading p_T jet. The inclusive Z background is shown after multiplying by a factor of 10^{-4}. For each plot we indicate the corresponding bin size in the y-axis label.

(1) *Pair Production Extraction cuts*
   (a) All the *Basic* cuts
   (b) $p_T(e^+/e^-) > 150$ GeV; $p_T(j_1) > 100$ GeV
   (c) $M(e^+, e^-) > 150$ GeV
   (d) $|M(e^+, j_k) - M_{e_8}| \leq 0.2M_{e_8}$ and $|M(e^-, j_l) - M_{e_8}| \leq 0.2M_{e_8}$ with $k \neq l = \{1, 2\}$.

In Fig. 10, L_D goes as L_{10} for both pair and combined productions, as in these cases the backgrounds become quite small compared to the signals. With the Discovery

TABLE II. The combined signal after Basic and Discovery cuts (see text for the definitions of the cuts) for $\Lambda = 5$ TeV and 10 TeV for different M_{e_8}.

M_{e_8}	$\Lambda = 5$ TeV		$\Lambda = 10$ TeV	
(GeV)	Basic (fb)	Discovery (fb)	Basic (fb)	Discovery (fb)
500	2.73 E4	1.31 E4	2.70 E4	1.27 E4
750	2.63 E3	1.93 E3	2.59 E3	1.91 E3
1000	442.95	367.20	415.35	347.16
1250	105.21	90.25	91.99	80.45
1500	31.73	27.25	24.54	21.86
1750	11.53	9.76	7.52	6.71
2000	4.77	3.92	2.59	2.28
2250	2.26	1.80	0.99	0.85
2500	1.18	0.91	0.42	0.36
2750	0.65	0.49	0.20	0.16
3000	0.37	0.27	0.11	0.08
3250	0.22	0.16	0.06	0.04
3500	0.13	0.09	0.03	0.02

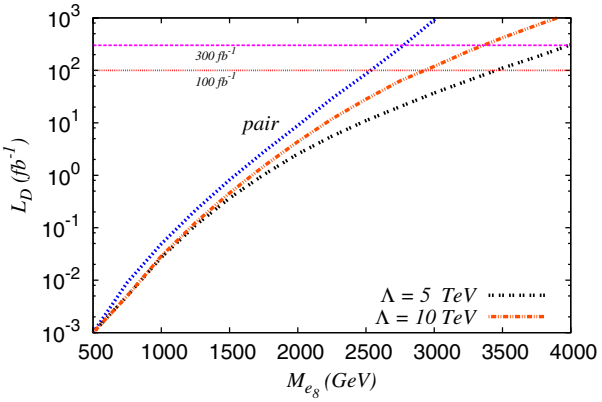

FIG. 10 (color online). The required luminosity for discovery (L_D) as a function of M_{e_8} with $\Lambda = 5$ and 10 TeV at the 14 TeV LHC for combined production with the Discovery cuts (see text for the definitions of the cuts). The L_D for pair production is computed after demanding that two e_8's be reconstructed instead of one.

cuts, the reach goes up to 3.4 and 2.9 TeV (4 and 3.3 TeV) with 100 fb^{-1} (300 fb^{-1}) integrated luminosity for $\Lambda = 5$ and 10 TeV, respectively, at the 14 TeV LHC. This also shows that for $\Lambda = 5$ TeV (10 TeV) with a combined signal at 14 TeV LHC with 300 fb^{-1} integrated luminosity, the reach goes up from the pair production by almost 1.2 TeV (0.5 TeV). However, we should keep in mind that this increase depends on Λ. As the single production cross section goes like $1/\Lambda^2$, if Λ is smaller than 5 TeV, then the reach of the combined production will increase even more, but for higher Λ (like $\Lambda = 10$ TeV, as shown in Fig. 10) its L_D plot will approach more towards the pair production plot.

V. SUMMARY AND CONCLUSIONS

In this paper we have studied the phenomenology of e_8's at the LHC and estimated the discovery potential of such particles at the LHC. We have explored various production channels of e_8's at the LHC, namely the pair, the two-body single, the three-body single and the indirect production channels. The contribution of the three-body single production channel is comparable to that of the two-body single production channel. While the pair production cross section dominates the other channels for low M_{e_8}, for high values of M_{e_8} the single productions become significant. The 14 TeV LHC with 100 fb^{-1} (300 fb^{-1}) of integrated luminosity can probe e_8's with masses up to 2.5 TeV (2.8 TeV) with only pair production. We have demonstrated how this reach can be increased further by combining signal events from different production processes. However, this increment is Λ dependent, as the single production cross section scales as $1/\Lambda^2$. For $\Lambda = 5$ TeV (10 TeV), the increment is about 0.9 TeV (0.4 TeV) with 100 fb^{-1} of integrated luminosity at the 14 TeV LHC, and with 300 fb^{-1} of integrated luminosity, it is about 1.2 TeV (0.5 TeV).

We point out that our analysis can also be used to probe Λ, the compositeness scale, for any fixed M_{e_8}. This is possible because of the scaling of the single production cross section with Λ. For example, for $M_{e_8} = 2$ TeV and $\Lambda = 10$ TeV, we estimate the single production cross section to be 1.2 fb, which we obtain from the events that pass the Discovery cuts but not the Pair Production Extraction cuts. By computing L_{10} (i.e., the luminosity requirement to observe ten signal events) from this, we can conclude that for $M_{e_8} = 2$ TeV, the 14 TeV LHC with 100 fb^{-1} (300 fb^{-1}) of integrated luminosity can probe $\Lambda \sim 35$ TeV (55 TeV). This can be useful, as the present searches of leptoquarks at the LHC generally focus on their pair production, which is mostly independent of Λ. However, even with the single production of leptoquarks at the LHC, it is difficult to probe the compositeness scale directly. This can be seen in an effective theory picture, as unlike leptogluons, the interaction Lagrangian of leptoquarks with the SM particles is dominated by renormalizable dimension-4 operators.

We note that the data from the current leptoquark searches at the LHC can be used to search for e_8's also. The current data for leptoquarks [10,11] already puts some constraints on the masses of the l_8's. For example, the data from the search for first-generation charged leptoquarks in the pair production channel clearly rules out a color octet electron of mass less than 900 GeV (see Fig. 10 of Ref. [10]), since the pair production cross section of color octet electrons is always larger than the pair production cross section of color triplet leptoquarks of the same mass due to color enhancement.[6]

ACKNOWLEDGMENTS

We thank J. Alwall and F. Maltoni for helping us with matching. S. M. thanks R. Barcelo for helpful comments.

APPENDIX: PREPARATION OF MATCHED SIGNAL

For the signal, we match the matrix element partons with the parton showers using the shower k_T scheme [30] in MADGRAPH5 with the matching scale $Q_{\rm cut} \sim 50$ GeV. We generate the combined signal including the different production processes as discussed in Sec. IV:

$$
\begin{aligned}
&pp \xrightarrow{e_8} ee \text{ (includes } P_{\rm ind}) \\
&pp \xrightarrow{e_8} ee + \text{1-j (includes } P_{\rm ind} + \text{1-j}, P_{2Bs}) \\
&pp \xrightarrow{e_8} ee + \text{2-j (includes } P_{\rm ind} + \text{2-j}, P_{2Bs} + \text{1-j}, P_{\rm pair}, P^3_{3Bs}) \\
&pp \xrightarrow{e_8} ee + \text{3-j (includes } P_{\rm ind} + \text{3-j}, P_{2Bs} + \text{2-j}, \\
&\quad P_{\rm pair} + \text{1-j}, P^3_{3Bs} + \text{1-j})
\end{aligned}
\tag{A1}
$$

where $P_{\rm pair}$, P_{2Bs}, P^3_{3Bs} and $P_{\rm ind}$ are the pair, two-body single, three-body single of the third type, and indirect productions, respectively. We refer the reader to Ref. [30] and the references therein for more details on the matching scheme and the procedure.

[6] After our paper was posted in the arXiv, a paper appeared [31] in which the authors estimate the exclusion limit of charged leptogluons from the CMS leptoquark data to be 1.2–1.3 TeV.

[1] G. Aad *et al.* (ATLAS Collaboration), Phys. Lett. B **716**, 1 (2012).
[2] S. Chatrchyan *et al.* (CMS Collaboration), Phys. Lett. B **716**, 30 (2012).
[3] J. C. Pati and A. Salam, Phys. Rev. D **10**, 275 (1974); **11**, 703(E) (1975).
[4] H. Terazawa, K. Akama, and Y. Chikashige, Phys. Rev. D **15**, 480 (1977).
[5] Y. Ne'eman, Phys. Lett. **81B**, 190 (1979).
[6] H. Harari, Phys. Lett. **86B**, 83 (1979).
[7] M. A. Shupe, Phys. Lett. **86B**, 87 (1979).
[8] H. Fritzsch and G. Mandelbaum, Phys. Lett. **102B**, 319 (1981).
[9] I. A. D'Souza and C. S. Kalman, *Preons: Models of Leptons, Quarks and Gauge Bosons as Composite Objects* (World Scientific, Singapore, 1992).
[10] S. Chatrchyan *et al.* (CMS Collaboration), Phys. Rev. D **86**, 052013 (2012).
[11] S. Chatrchyan *et al.* (CMS Collaboration), Phys. Rev. Lett. **110**, 081801 (2013).
[12] G. Aad *et al.* (ATLAS Collaboration), Phys. Rev. D **85**, 072003 (2012).
[13] T. G. Rizzo, Phys. Rev. D **33**, 1852 (1986).
[14] T. G. Rizzo, Phys. Rev. D **34**, 133 (1986).
[15] K. H. Streng, Z. Phys. C **33**, 247 (1986).
[16] A. Celikel and M. Kantar, Turk. J. Phys. **22**, 401 (1998).
[17] J. L. Hewett and T. G. Rizzo, Phys. Rev. D **56**, 5709 (1997).
[18] A. Celikel, M. Kantar, and S. Sultansoy, Phys. Lett. B **443**, 359 (1998).
[19] M. Sahin, S. Sultansoy, and S. Turkoz, Phys. Lett. B **689**, 172 (2010).
[20] A. N. Akay, H. Karadeniz, M. Sahin, and S. Sultansoy, Europhys. Lett. **95**, 31001 (2011).
[21] J. Beringer *et al.* (Particle Data Group), Phys. Rev. D **86**, 010001 (2012).
[22] F. Abe *et al.* (CDF Collaboration), Phys. Rev. Lett. **63**, 1447 (1989).
[23] U. Baur and K. H. Streng, Phys. Lett. **162B**, 387 (1985).
[24] W. Bartel *et al.*, Z. Phys. C **36**, 15 (1987).
[25] I. Abt *et al.* (H1 Collaboration), Nucl. Phys. **B396**, 3 (1993).
[26] N. D. Christensen and C. Duhr, Comput. Phys. Commun. **180**, 1614 (2009).
[27] C. Degrande, C. Duhr, B. Fuks, D. Grellscheid, O. Mattelaer, and T. Reiter, Comput. Phys. Commun. **183**, 1201 (2012).
[28] J. Alwall, M. Herquet, F. Maltoni, O. Mattelaer, and T. Stelzer, J. High Energy Phys. 06 (2011) 128.
[29] J. Pumplin, D. R. Stump, J. Huston, H. L. Lai, P. M. Nadolsky, and W. K. Tung, J. High Energy Phys. 07 (2002) 012.
[30] J. Alwall, S. de Visscher, and F. Maltoni, J. High Energy Phys. 02 (2009) 017.
[31] D. Goncalves-Netto, D. Lopez-Val, K. Mawatari, I. Wigmore, and T. Plehn, arXiv:1303.0845.